11A. 2 INCLUDING THE ENVIRONMENTAL WIND EFFECTS ON SMOKE PLUME RISE OF VEGETATION FIRES IN 1D CLOUD MODELS

S. R. Freitas *

Center for Weather Forecasting and Climate Studies, INPE, Cachoeira Paulista, Brazil

K. M. Longo

Center for Space and Atmospheric Sciences, INPE, São José dos Campos, Brazil

J. Trentmann

University of Mainz, Mainz, Germany (Now at German Weather Service, Offenbach, Germany)

D. Latham

USDA Forest Service, Montana, USA

ABSTRACT

We revisit the parameterization of the vertical transport of hot gases and particles emitted from biomass burning, described in Freitas et al. (2007), to include the effects of environmental wind on transport and dilution of the smoke plume at the cloud scale. Typically, the final vertical height that the smoke plumes reaches is controlled by the thermodynamic stability of the atmospheric environment and the surface heat flux released from the fire. However, in presence of strong horizontal wind, it might enhance the lateral entrainment and induces an additional drag, particularly for small fires, impacting the injection height. This process is quantitatively represented by introducing an additional entrainment term to represent the organized inflow of the cooler and drier ambient air into the plume and its drag by the momentum transfer. An extended set of equations including the horizontal motion of the plume and the additional increase of the plume radius size is now solved to explicitly simulate the time evolution of the plume rise. One-dimensional (1D) model results are presented for two hypothetical deforestation fires in the Amazon basin with sizes of 10 and 50 ha and under calm and windy environments. The results are then confronted with corresponding simulations generated by the complex non-hydrostatic 3D Active Tracer High resolution Atmospheric Model (ATHAM). We show that the 1D model can generate feasible comparisons with the fully 3D simulations.

1 INTRODUCTION

Biomass burning emits hot gases and particles which are transported upward with the positive buoyancy of the fire. Due to radiative cooling and the efficient heat transport by convection, there is a rapid decay of temperature above the fire area. Also, the interaction between the smoke and the environment produces eddies that entrain colder environmental air into the smoke plume, which dilutes the plume and reduces buoyancy. The dominant characteristic is a strong upward flow with an only moderate temperature excess from the ambient. The final height that the plume reaches is controlled by the thermodynamic stability of the atmospheric environment and the surface heat flux release from the fire. Moreover, if water vapor is allowed to condense, the additional buoyancy gained from latent heat release plays an important role in determining the effective injection height of the plume. However, the occurrence of strong horizontal wind might enhance the lateral entrainment and even prevent the plume to reach the condensation level, particularly for small fires, impacting the injection height. Figure 1 illustrates the ambient wind effects on the smoke plume rise. This figure shows two photographs of the smoke plume rise produced from two different deforestation fires in the Amazon basin. On the left side case, the plume moves upward with a slight bent-over indicating its development in a calm environment. However, the plume of the right side case shows much stronger deflection from the local vertical direction, an indicative of windy environment. Also note that both plumes are capped by cumulus, what indicates that cloud microphysics might have had a significant role on the plume rise development. Note that size of the fires and the plume height

* *Corresponding author address:* Saulo R. Freitas, Center for Weather Forecasting and Climate Studies, INPE, Cachoeira Paulista, Brazil, e-mail: saulo.freitas@cptec.inpe.br

Figure 1. Two photographs of the smoke plume rise produced from two different deforestation fires in the Amazon basin (Pictures taken by M.O. Andreae and M. Welling.)

differs substantially between both plumes.

The effect of the ambient wind on the plume rise development from volcanoes sources has been studied by several authors. Graf et al. (1999) performed a set of sensitivity studies using a two-dimensional version of the Active Tracer High resolution Atmospheric Model as a non-hydrostatic volcano plume model. The authors applied this modeling system to simulate the impacts of environmental conditions on the vertical plume development. They found that, in general, the horizontal wind reduces the height reached by the plume as well as the static stability play a role on that. Moreover, all environmental impacts strongly depend on the intensity of the air entrainment into the plume. Bursik (2001) applied a 1D theoretical model of a plume to study the interaction between a volcanic plume and ambient wind. He also shows that the enhanced entrainment decreases the plume rise height mainly in altitudes with high wind speeds of the polar jet.

In this paper we revisit a 1D parameterization of the vertical transport emissions from vegetation fires, described in Freitas et al. (2007, hereafter F2007), to include the effects of environmental wind on transport and dilution of the smoke plume at the cloud scale. This process is quantitatively represented by introducing an additional entrainment term to represent the organized inflow of the ambient air into the plume, as well as its drag by the external ambient wind. The extra entrainment enhances the in-cloud mixing with the cooler and drier ambient air. The net effect on the dynamics is a reduction of the in-cloud velocity on the vertical direction by transferring momentum to the entrained air mass; while horizontally, there is a strong acceleration in the nearby surface layer as well as in the layers with strong ambient wind shear. An extended set of equations, including the horizontal motion of the plume and the additional increase of the plume size, is now solved to explicitly simulate the time evolution of the plume rise and determine the final injection layer. This information can then be used to determine the verticals layers of 3D low resolution atmospheric chemistry-transport models, where trace gases and aerosols emitted during the flaming phase of the vegetation fires are released, transported and dispersed.

This paper is organized as follows. In section 2, the methodology is described. Section 3, part 1 discusses the dynamic and thermodynamical situation of the cases studies. Then, the numerical simulations with 3D ATHAM and the 1D plume models are introduced and confronted. Our conclusions are discussed in section 4. Biomass burning and some estimated plume rise characteristics

2 METHODOLOGY

The smoke plume rise associated to the biomass burning is explicitly simulated using a simple one-dimensional time-dependent entrainment plume model (Latham, 1994; F2007; hereafter 1D PRM). The Eqs. (1) to (7) reintroduce the 1D PRM, including now the horizontal ambient wind effect (news terms and equations are wrote in blue color):

$$\frac{\partial w}{\partial t} + w\frac{\partial w}{\partial z} = \frac{1}{1+\gamma} gB - \frac{2\alpha}{R} w^2 - \delta_{entr} w \quad (1)$$

$$\frac{\partial T}{\partial t} + w\frac{\partial T}{\partial z} = -w\frac{g}{c_p} - \frac{2\alpha}{R}|w|(T - T_e) - \delta_{entr}(T - T_e) + \left(\frac{\partial T}{\partial t}\right)_{micro-physics} \quad (2)$$

$$\frac{\partial r_v}{\partial t} + w\frac{\partial r_v}{\partial z} = -\frac{2\alpha}{R}|w|(r_v - r_{ve}) - \delta_{entr}(r_v - r_{ve}) + \left(\frac{\partial r_v}{\partial t}\right)_{micro-physics} \quad (3)$$

$$\frac{\partial r_c}{\partial t} + w\frac{\partial r_c}{\partial z} = -\frac{2\alpha}{R}|w|r_c - \delta_{entr}r_c + \left(\frac{\partial r_c}{\partial t}\right)_{micro-physics} \quad (4)$$

$$\frac{\partial r_{ice,rain}}{\partial t} + w\frac{\partial r_{ice,rain}}{\partial z} = -\frac{2\alpha}{R}|w|r_{ice,rain} - \delta_{entr}r_{ice,rain} + \left(\frac{\partial r_{ice,rain}}{\partial t}\right)_{micro-physics} + \mathbf{sedim}_{ice,rain} \quad (5)$$

$$\frac{\partial u}{\partial t} + w\frac{\partial u}{\partial z} = -\frac{2\alpha}{R}|w|(u - u_e) - \delta_{entr}(u - u_e) \quad (6)$$

$$\frac{\partial R}{\partial t} + w\frac{\partial R}{\partial z} = +\frac{6\alpha}{5R}|w|R + \frac{1}{2}\delta_{entr}R \quad (7)$$

Here w, T, r_v, r_c, r_{rain}, r_{ice} are the vertical velocity, air temperature, water vapor, cloud, rain and ice mixing ratios, respectively, and are associated to in-cloud air parcels. The velocity u represents the center of mass horizontal velocity of the plume in a given level z. In the equations above the index e stands for the environmental value. The lateral entrainment coefficient is based on the traditional formulation $2\alpha R^{-1}$, where R stands for the radius of the plume and α = 0.05. In a windy ambient, the relative horizontal motion between the plume and the ambient air enhances the lateral entrainment through a 'collisional' process promoting an additional exchange of momentum, energy, water, trace gases and aerosols between both bodies. We assume instantaneous mixing between in-cloud and ambient properties inside the plume. To quantitatively include this process, we add an extra entrainment term called 'dynamic entrainment' (δ_{entr}) formulated as

$$\delta_{entr} = \frac{2}{\pi R}(u_e - u), \quad (8)$$

where all variables were previously defined. One should note that the dynamic entrainment is proportional to the difference between the magnitudes of the ambient and plume air horizontal velocities, which means no extra entrainment when both bodies are moving at the same speed, as expected. Also, δ_{entr} is inversely proportional to the plume radius size meaning that bigger the plume less sensitive it is to this entrainment process. The derivation of Eq. (8) is given as follows. Considering a cylinder volume of radius R and depth Δz (see Figure 2), the in-cloud horizontal mass flux (f_h) is given by (kg m^{-2} s^{-1})

$$f_h = \rho_{env}(u_e - u)$$

where ρ_{env} is the ambient air density and u_e and u were already defined. Therefore, the mass gained by this cloud layer during the time Δt is

$$\Delta m = f_h(2R\Delta z)\Delta t = \rho_{env}(u_e - u)(2R\Delta z)\Delta t$$

The definition of the mass entrainment rate is

$$\delta_{entr} = \frac{1}{m}\frac{\Delta m}{\Delta t} = \frac{1}{\pi R^2 \Delta z \rho_{cloud}}\frac{\rho_{env}(u_e - u)(2R\Delta z)\Delta t}{\Delta t}$$

where ρ_{cloud} is the in-cloud air density. Assuming that

$$\rho_{cloud} \approx \rho_{env},$$

We finish with the Eq. (8) for the dynamic entrainment.

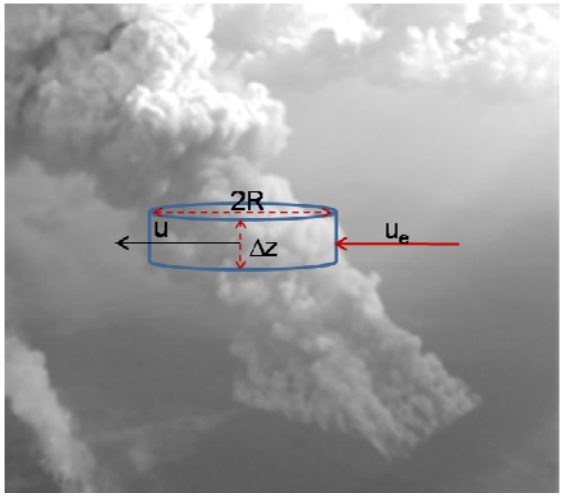

Figure 2 The derivation the dynamic entrainment rate formulation (picture taken by M. Welling).

Eq. (1) is the vertical equation of motion. The new term ($-\delta_{entr} w$) expresses the loss rate of in-cloud vertical velocity due momentum transfer to the ambient air mass entrained into the plume (environmental vertical velocity is supposed be negligible when comparing with the in-cloud vertical velocity). Eqs. (2) – (5) express the first law of thermodynamics and mass continuity equations for water phases including the dynamic entrainment process. This process is included using the traditional bulk formulation, being expressed by the product of the entrainment rate and the difference between in-cloud and ambient values. For more details of, see F2007. Eq. (6) is introduced to represent the gain of horizontal velocity of the plume due its drag by the ambient air. The entrainment terms are responsible for the bent-over plumes. The lower boundary condition for the solution (u) of this equation is $u(z=0)=0$. From Eq. (6), the former lower boundary condition and in an ambient at rest ($u_e(z)=0$), the plume will develop only vertical motion, reducing to the original solution of F2007. Eq. (7) represents the increase of plume radius size due the entrainment processes; in this case amplified by the organized inflow of ambient air into the plume. In ambient at rest, Eq. (7) reduces to the traditional Turner style plume (Turner, 1973; Latham, 1994). The lower boundary condition for the solution of Eq. (7) is obtained from the fire size.

3 CASES STUDIES AND 1D PRM COMPARISONS WITH THE ATHAM MODEL

3.1 *Description of the cases studies*

To evaluate model performance and sensitivity to the different environmental conditions, we performed a set of numerical experiments using two selected termodynamical situations. Figure 3 shows the two cases obtained from rawinsondes launched in the burning season of 2002 in the Amazon basin over a Forest site and close to deforestation areas. Figure 3 (A) depicts a typical atmospheric condition on Amazon basin and central part of South America during the burning season at 1800Z, normally the peak time of the diurnal cycle of the number of fires. The rawinsonde, launched around 1800Z on 20 September 2002, shows a strong thermal inversion around 800 hPa with a very dry layer above, this was labeled as the dry case. On the other side, the situation described by the rawinsonde launched one week later and on the same region Figure 3 B) is quite different. There was a weaker thermal inversion around 870 hPa and a much moister layer above compared with the former case, this was classified as the wet case. In addition, these two cases also presented a significant different on the horizontal wind magnitude (see Figure 3 C). For the dry case, the mean magnitude is around 2 m s^{-1} from surface to 500 hPa while the wet case has values around 4 to 5 m s^{-1}. Note also the strong wind shear in the first 1500 m for both situations, from ~2 to 4 m s^{-1} and ~2 to 6 m s^{-1} for dry and wet cases, respectively.

3.2 *ATHAM model runs*

The active tracer high resolution atmospheric model (Oberhuber et al., 1998) is a three-dimensional atmospheric plume model, which has been designed and employed for the simulation of strong convective events, e.g., volcanic eruptions (e.g., Graf et al., 1999; Herzog et al., 2003; Textor et al., 2003) and vegetation fires (e.g., Trentmann et al., 2002, 2006; Luderer et al., 2006). ATHAM solves the Navier-Stokes equation for a gas-particle mixture based on external forcings including the transport of active tracers and cloud microphysical processes (Textor et al., 2006). Fire emissions are represented in ATHAM by prescribed emission fluxes of heat, moisture and aerosol particles into the lowest atmospheric model layer. The model simulations presented here were conducted

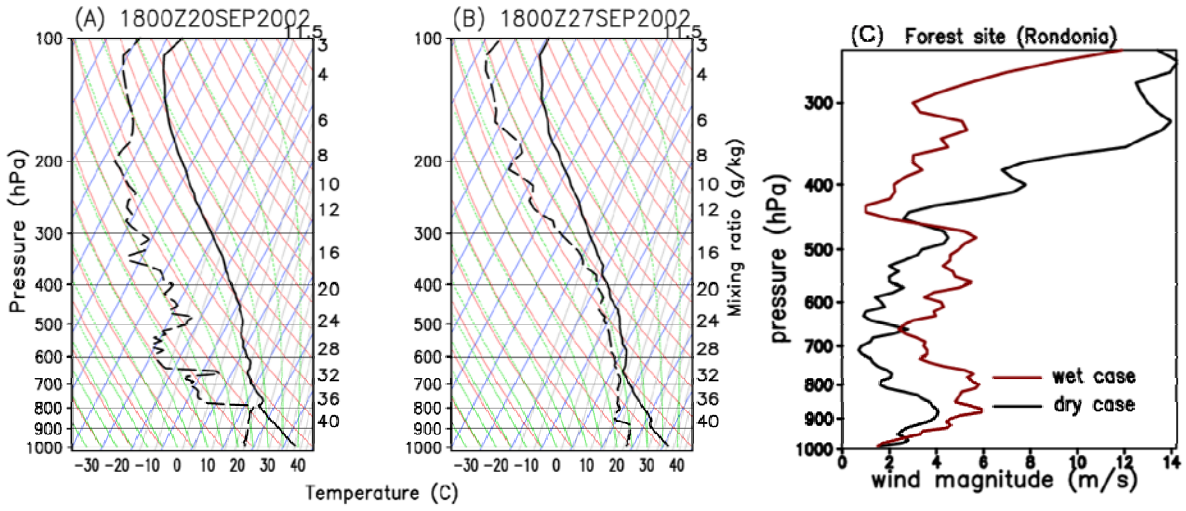

Figure 3. Temperature (solid) and dew point temperature (dashed) profiles from rawinsonde launched in Rondonia (11S, 60W) shown with a skew T – log p diagram. Case (A) depicts the condition around 1800Z on 20 September 2002, classified as the dry case. (B) is the wet case corresponding to around 1800Z on 27 September 2002 (reproduced from Freitas et al., 2007). (C) Horizontal wind magnitude profiles of the dry (black) and wet (red) cases obtained from the rawinsondes.

on a stretched grid with a minimum horizontal and vertical model grid spacing of 50 m x 50 m x 50 m in the center and increasing grid spacing towards the edges of the model domain. The total model domain covered 15 km x 15 km x 23 km. The maximum time step was set to 1.5 s, the minimum time step was determined dynamically by the CFL criterion. The heat flux and its temporal evolution were set accordingly to the 1D PRM model.

Figure 4 presents the horizontally averaged aerosol mass distributions at different times after model start for a fire with a size of 10 ha and a heat flux of 80 kW m^{-2} for the dry (panel A) and the wet cases (panel B). The main simulated outflow height of the dry case is slightly below 4 km, while the outflow height of the wet case is at around 1.5 km. The differences in the outflow height are determined by the different thermodynamical stabilities of the profiles (Figure 4 A and B) and the differences in the wind profiles (see Figure 4 C) with a stronger horizontal wind in the wet case. In Figure 4 (B) results from four simulation times are presented demonstrating that the emission height reaches an equilibrium level after 30 minutes of simulation.

Figure 4, panels (C) and (D), shows the corresponding results from ATHAM simulations assuming a fire with a size for 50 ha. As expected, in both cases the emission height reaches higher altitudes than in the case of the 10 ha fire. The thermodynamical structures of the profiles result in a narrow altitudinal distribution of the aerosol distribution in the wet case around 4 km, while the aerosol is spread between 4 and 6 km in the dry case.

3.3 *1D PRM model runs*

The 1D PRM ran using constant grid space resolution of 100 m with top at 20 km height. The model time step was dynamically calculated following the CFL stability criterion, not exceeding 5 s. The microphysics is resolved with time splitting (1/3 of dynamic timestep). The upper boundary condition is defined by a Rayleigh friction layer with 60 s timescale. To convert the heat flux to convective energy, the McCarter and Broido (1965) factor (0.55) is used. The environmental condition for air pressure, temperature, water vapor mixing ratio, horizontal velocity and density were provided by the two rawinsondes described at Section 3.1. Fire sizes of 10 and 50 ha were defined for the model simulations. Typically, the steady state is reached within 50 min, this number being the upper limit of the time integration. The final rise of the plume is determined by the height which the vertical velocity of the in-cloud air parcel is less than 1m s^{-1}.

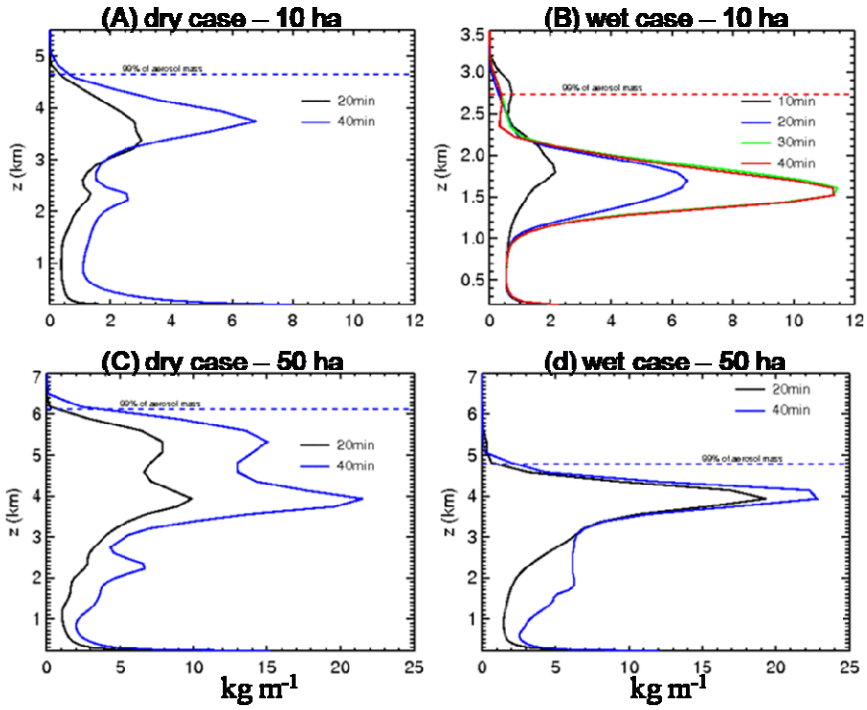

Figure 4. Horizontally averaged aerosol mass distribution (kg m^{-1}) as simulated by ATHAM model for the dry (A, C) and wet (B, D) cases. Model results for a fire with size of 10 ha (A, B) and 50 ha (C, D). All simulations used a heat flux of 80 kW m^{-2}.

3.4 *1D PRM and ATHAM simulations comparison*

Figure 5 (A) and (B) show the 1D PRM model steady state solution for the dry and wet cases, respectively, for fires on forest biome with a heat flux of 80 kW m^{-2} and fire size of 10 ha. The vertical velocity (W, m s^{-1}) and vertical mass distribution (VMD %) profiles are shown. VMD definition is based on ATHAM simulated features and expresses the probably mass distribution as a function of the vertical velocity profile simulated by 1D PRM. ATHAM model results for the vertical velocity profiles (not shown) demonstrated that the main smoke injection layer, defined in terms of the horizontally averaged mass distribution (see Figure 4), is fairly situated in the upper half part of the cumulus. The upper part is defined from the vertical level where the in-cloud vertical velocity starts to decrease until it vanishes. Based on this information, the vertical mass distribution is defined as follow:

a) from the 1D PRM steady state vertical velocity profile, the upper half part of the cumulus is determined in terms of the heights Zi and Zf (Zf > Zi);

b) a parabolic function of the height Z with roots at Zi and Zf is defined;

c) the function is then normalized to 1 in the interval [Zi, Zf].

For both cases, we also performed a run considering a hypothesis of an ambient at rest. For the dry case, Figure 5 (A), 1D PRM prognoses a cloud top around 4 and 5 km including or not the ambient wind effect (AWE), respectively. Thus, in this case, the enhanced entrainment reduced the cloud top by around 1 km. The cloud top predicted by ATHAM (Figure 4 A) was ~ 4.8 km with the aerosol mass detrainment layer localized approximately between 3 and 4.5 km (showed at Figure 5 as a grey filled rectangles). Our VMD definition with the AWE turned off coincides well with the ATHAM results, being however broader. Including the AWE, 1D PRM prognoses a lower layer, with approximately the upper half inside the ATHAM zone and the lower half below that. Figure 5 (C) shows total condensate water (**CW**), buoyancy acceleration ($\mathbf{B_a}$) and entrainment acceleration ($\mathbf{E_a}$) for the case discussed before. Not including the AWE, the plume is capped by a cumulus with the CW of ~ 2 g kg^{-1} at 5 km height. AWE strongly reduces the cumulus, not only the **CW** (maximum ~ 1 g kg^{-1}) but also its volume. For the forcing terms of vertical equation of motion (Eq. 1), it can be noted a reduction of the $\mathbf{B_a}$ due the enhanced

entrainment of drier air. On the other hand, $\mathbf{E_a}$ is increased in the lower levels, due to additional dynamic entrainment. At upper vertical levels, $\mathbf{E_a}$ decreases given that δ_{entr} is smaller (because $\boldsymbol{u}$ is approximately $\boldsymbol{u_e}$) and at the same time the lateral entrainment is smaller due to larger $\boldsymbol{R}$.

The wet and windy case is discussed as follow. Profiles of W and VMD are shown in Figure 5 (B). Including or not the AWE, results on sharply differences, as it can be noted. The cloud top predicted by ATHAM (Figure 4 B) was ~ 2.5 km with the aerosol mass detrainment layer localized approximately between 1 and 2.3 km. Not including AWE results on a fully disagreement between 1D PRM cloud top and VMD with ATHAM. The predicted cloud top is at ~ 5.8 km with a VMD between 2.8 and 5.8 km, well far of ATHAM results. Including the AWE, 1D PRM prognoses a much lower cloud top at ~ 2.6 km with a VMD between 1 and 2.5 km. The agreement with ATHAM is now significantly improved. For this case, **CW,** $\mathbf{B_a}$ and $\mathbf{E_a}$ are showed at Figure 5 (D). Because the ambient air is moister in this case, not including the AWE, the plume is capped by a bigger cumulus with the **CW** of ~ 4 g kg^{-1} at 5.5 km height. However, because of the stronger deceleration caused by δ_{entr} due to windy environment in this case, the plume is prevented to reach the condensation level. No clouds are formed at top of the plume (**CW** ~ 0) and, consequently, there is no additional buoyancy gained from latent heat release. Both processes explain the much lower 'cloud' top and injection layer presented in this situation.

Figure 5 (F – I) introduces the results for bigger fires with size of 50 ha. All others settings remain the same as described before. The larger size of the fire promotes stronger updrafts and higher clouds tops, similar to ATHAM results. The dry case is showed in panel (F) for W and VMD profiles. The inclusion of AWE reduces the cloud top by 1 km (from 7 to 6 km). The cloud top predicted by ATHAM (Figure 4 C) was ~ 6 km with the aerosol mass detrainment layer localized approximately between 3 and 5.8 km. The results of the 1D PRM with AWE presents a better agreement with ATHAM simulation in terms of the predicted cloud top as well as the injection layer height and depth, as described by the VMD quantity. Figure 5 (G) shows the results for the wet and windy case. As in the case for fire size of 10 ha discussed before, including AWE causes larger changes in the simulated plume rise, the cloud top drops from 8.5 to 5.8 km in this case. The VMD without AWE is centered on 6.5 km extending from 4 to 8.5 km. Including AWE, VMD center drops to 4.2 km and extends from 2.8 to 5.8 km. From ATHAM simulation (Figure 4 D), the predicted cloud of this case is around 4.9 km with the main detrainment aerosol layer localized between ~ 2.9 and 4.9 km. Therefore, including the additional entrainment from the ambient wind results on a much better agreement with ATHAM simulated features, as well as in the dry case. 1D PRM results and discussion of the simulated **CW,** $\mathbf{B_a}$ and $\mathbf{E_a}$ for the 50 ha fire are very similar to the presented for the 10 ha fire size and are shown at panels (H) and (I). Although the simulation of the plume developed in wet and windy ambient (panel I) also is capped by a cumulus, indicating that even in this case the plume can reach the condensation level due the stronger initial updraft associated to the larger fire size.

4 CONCLUSIONS

We have extended the 1D cloud model described in F2007 to include the effect of the ambient wind on the smoke plume rise development associated to vegetation fires. This process is represented as an additional entrainment term proportional to the difference between horizontal wind speeds of the center of mass of the plume and the ambient air. We have shown that this effect has important impact on the definition of the cloud top and detrainment mass layer mainly for smaller fires under moist and windy situations. To verify the reliability of the physical representation of 1D model, its results are compared with ones produced using the complex non-hydrostatic 3D ATHAM model. Our findings suggest that the extended 1D model can generate feasible simulations when compared with the 3D model results.

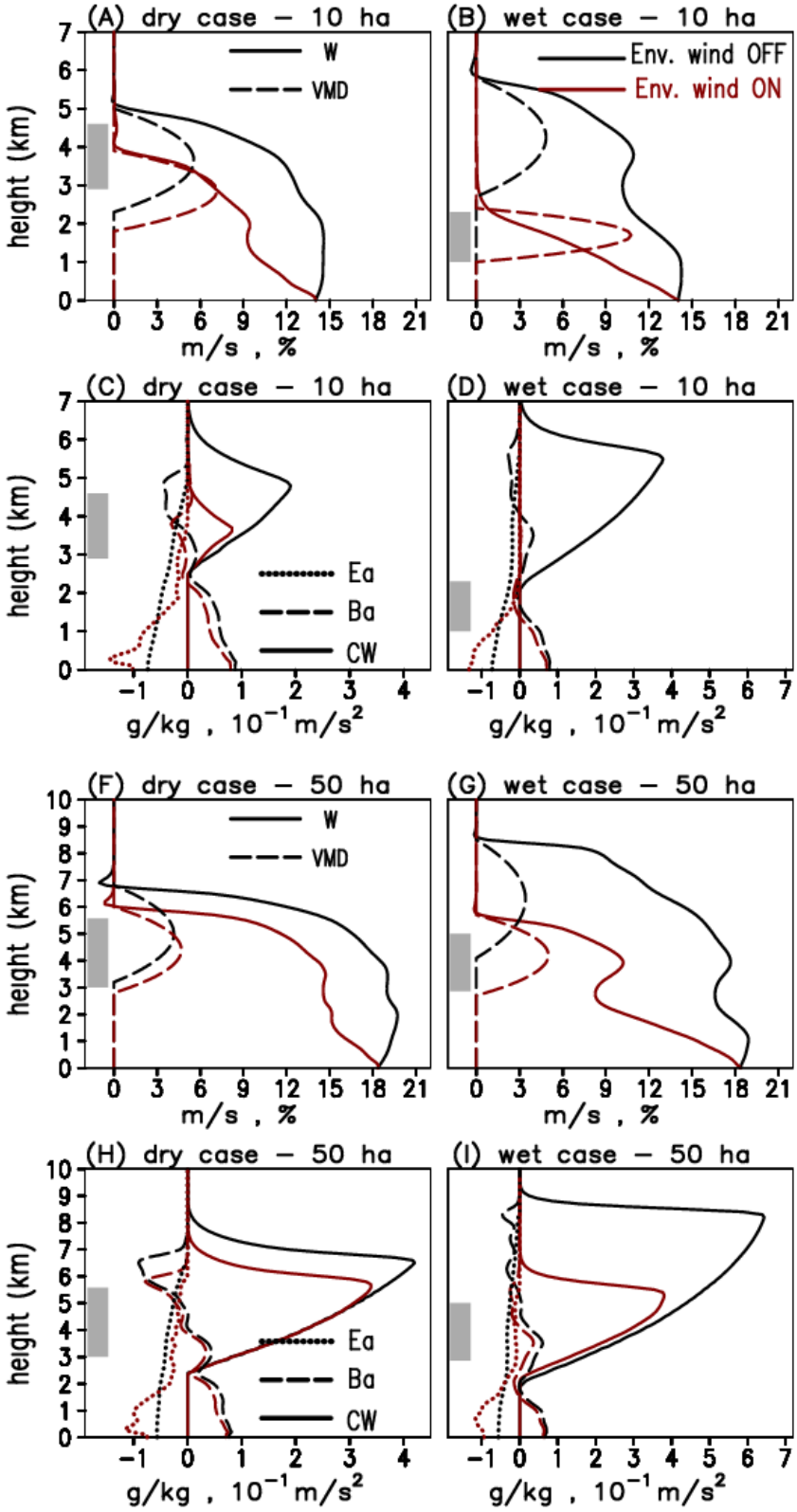

Figure 5. Plume model steady state solution for the dry (fire size of 10 ha: A and C; 50 ha: F and H) and wet (fire size of 10 ha: B and D; 50 ha: G and I) and heat flux of 80 kW m^{-2}. The quantities are: vertical velocity (**W**, m s^{-1}), vertical mass distribution (**VMD**, %), entrainment acceleration (**Ea**, 10^{-1} m s^{-2}), buoyancy acceleration (**Ba**, 10^{-1} m s^{-2}) and total condensate water (**CW**, g kg^{-1}). Model results considering the actual ambient wind are in red and the ambient at rest in black colors. The grey rectangles indicate the main injection layer simulated by ATHAM model.

ACKNOWLEDGEMENTS

We acknowledge partial support of this work by CNPq (302696/2008-3, 309922/2007-0) and by the Max Planck Society (MPG). JT thanks Stephan Eto for conducting the ATHAM model.

REFERENCES

Bursik, M. (2001), Effect of wind on the rise height of volcanic plumes, *Geophys. Res. Lett.*, 28(18), 3621–3624.

Freitas, S. R., K. M. Longo, R. Chatfield, D. Latham, M. A. F. Silva Dias, M. O. Andreae, E. Prins, J. C. Santos, R. Gielow, and J. A. Carvalho Jr. (2007), Including the sub-grid scale plume rise of vegetation fires in low resolution atmospheric transport models, *Atmospheric Chemistry and Physics*, v. 7, p. 3385-3398.

Graf, H.-F, M. Herzog, J. M. Oberhuber, and C. Textor (1999), The effect of environmental conditions on volcanic plume rise*, J. Geophys. Res.,* 104(D20), 24309-24320.

Herzog, M., J. M. Oberhuber, and H.-F. Graf (2003), A Prognostic Turbulence Scheme for the Nonhydrostatic Plume Model ATHAM, *J. Atmos. Sci*., 60, 2783-2796.

Latham, D. (1994), PLUMP: A one-dimensional plume predictor and cloud model for fire and smoke managers, General Technical Report INT-GTR-314, Intermountain Research Station, USDA Forest Service.

Luderer, G., J. Trentmann, T. Winterrath, C. Textor, M. Herzog, and M. O. Andreae (2006), Modeling of biomass smoke injection into the lower stratosphere by a large forest fire (Part II): Sensitivity studies, *Atmos. Chem. Phys*., 6, 5261–5277.

McCarter, R., and A. Broido (1965), Radiative and convective energy from wood crib fires, *Pyrodinamics*, 2, 65-85.

Oberhuber, J., M. Herzog, H.-F. Graf, and K. Schwanke (1998), Volcanic plume simulation on large scales, *J. Volcanol. Geotherm. Res.*, 87, 29–53.

Textor, C., H.-F. Graf, M. Herzog, and J. M. Oberhuber (2003), Injection of gases into the stratosphere by explosive volcanic eruptions, *J. Geophys. Res*., 108(D19), 4606, doi:10.1029/2002JD002987.

Textor, C., H. F. Graf, M. Herzog, J. Oberhuber, W. I. Rose, and G. G. J. Ernst (2006a), Volcanic particle aggregation in explosive eruption columns. Part I: Parameterization of the microphysics of hydrometeors and ash, *J. Volcanol. Geotherm. Res*., 150, 359–377.

Trentmann J., M. O. Andreae, H.-F. Graf, P. V. Hobbs, R. D. Ottmar, and T. Trautmann (2002), Simulation of a biomass-burning plume: Comparison of model results with observations*, J. Geophys. Res*., 107 (D2), 4013, doi:10.1029/2001JD000410.

Trentmann, J., G. Luderer, T. Winterrath, M. Fromm, R. Servranckx, C. Textor, M. Herzog, and M. O. Andreae (2006), Modeling of biomass smoke injection into the lower stratosphere by a large forest fire (Part I): Reference study*, Atmos. Chem. Phys*., 6, 5247–5260.

Turner, J. S. (1973), Buoyancy effects in fluids, Cambridge Univ. Press, Cambridge, 368 pp.